EFDA–JET–PR(14)13

R. Dejarnac, A. Podolnik, M. Komm, G. Arnoux, J.W. Coenen,
S. Devaux, L. Frassinetti, J.P. Gunn, G.F. Matthews, R.A. Pitts
and JET EFDA contributors

Numerical Evaluation of Heat Flux and Surface Temperature on a Misaligned JET Divertor W-Lamella During ELMs

Numerical Evaluation of Heat Flux and Surface Temperature on a Misaligned JET Divertor W-Lamella During ELMs

R. Dejarnac[1], A. Podolnik[1,2], M. Komm[1], G. Arnoux[3], J.W. Coenen[4], S. Devaux[5], L. Frassinetti[6], J.P. Gunn[7], G.F. Matthews[3], R.A. Pitts[8] and JET EFDA contributors*

JET Joint Undertaking, Culham Science Centre, OX14 3DB, Abingdon, UK

[1]*Institute of Plasma Physics, AS CR v.v.i., Prague, Czech Republic*
[2]*MFF Charles University, V Holešovičkách 2, 180 00 Prague, Czech Republic*
[3]*Euratom/CCFE, Culham Science Center, Abingdon OX14 3DB, UK*
[4]*Institute of Energy and Climate Research – Plasma Physics, Forschungszentrum Juelich, Germany*
[5]*Max-Plank-Institute for Plasma Physics, Euratom Association, Garching, Germany*
[6]*Division of Fusion Plasma Physics, KTH, SE-10044 Stockholm, Sweden*
[7]*CEA, IRFM, F-13108 Saint-Paul-lez-Durance, France*
[8]*ITER Organization, Route de Vinon sur Verdon, 13115 St Paul-lez-Durance, France*
** See annex of F. Romanelli et al, "Overview of JET Results", (24th IAEA Fusion Energy Conference, San Diego, USA (2012)).*

Preprint of Paper to be submitted for publication in
Nuclear Fusion

ABSTRACT

A series of experiments has been performed on JET to investigate the dynamics of transient melting due to Edge Localized Modes (ELMs). The experiment employs a deliberately misaligned lamella in one module of the JET bulk tungsten outer divertor, allowing the combination of stationary power flux and ELMs to transiently melt the misaligned edge. During the design of the experiment a number of calculations were performed using 2D particle-in-cell (PIC) simulations and a heat transfer code to investigate the influence on the deposited power flux of finite Larmor radius effects associated with the energetic ELM ions. This has been performed using parameter scans inside a range of pedestal temperatures and densities to scope different experimentally expected ELM energies. On one hand, we observe optimistic results, with smoothing of the heat flux due to the Larmor gyration on the protruding side of the lamella which sees the direct parallel flux – the deposited power tends to be lower than the nominal value expected from geometric magnetic field line impact over a distance smaller than 2 Larmor radii, a finding which is always valid during ELMs for such a geometry. On the other hand, the fraction of the flux not reaching the directly wetted side is transferred and spread to the top surface of the lamella. The hottest point of the lamella (corner side/top) does not always benefit from the gain from the Larmor smoothing effect because of an enhanced power deposition from the second contribution.

1. MOTIVATIONS

Tungsten is the material chosen to armour the ITER divertor. The energy stored in a typical ITER discharge achieving $Q_{DT} = 10$ in H-mode with15 MA of plasma current will be 350MJ [1]. Part of this energy will be periodically released in very short bursts during Edge Localized Modes (ELMs) in the form of particle and heat fluxes. Power fluxes reaching metallic plasma-facing components (PFC) during ELMs or other transient events may exceed material limits if they cannot be mitigated and can lead to melting [2–6]. In order to assess the melting of metallic objects in tokamaks and its consequences, the fusion community has recently directed considerable effort into dedicated experiments and numerical modeling of melt dynamics and the effect of melting on tokamak operations. The AUG and JET tokamaks changed their divertor PFCs from graphite/CFC to CFC coated W or bulk W [7–10] and Tore Supra is now changing to a full metallic machine with the WEST project [11].

Usually, PFCs which have the strongest interaction with the plasma have surfaces oriented with glancing angles to the magnetic field in order to spread the power over the widest possible area. However, in these high flux regions, the components are generally castellated in order to withstand thermo-mechanical stress. The risk of melting comes mainly from edges due to mechanical misalignment between components. At these edges, the plasma impacts at near normal incidence on the material and deposited heat fluxes can increase by more than one order of magnitude compared with the front surface values. Using kinetic simulations, it has recently been shown, however, that in the case of high energy ions (such as those impacting on PFCs during ELM transients), the heat

flux onto edges perpendicular to magnetic field lines can be reduced from the values expected geometrically as a result of Larmor radius induced smoothing effects [12]. This reduction operates over a distance roughly equal to two Larmor radii (r_L).

To study the dynamics and consequences of transient melting in support of the decision to use tungsten in the ITER divertor, a dedicated experiment was performed on JET tokamak in the summer 2013. A specially designed tungsten lamella, protruding with respect to its neighbours, was implemented in the JET bulk W outer divertor. The lamella was exposed to high power fluxes during a short time by moving the outer divertor strike point onto the protruding edge for a short time (~1.5s) during high power ELMing H-mode JET pulses [13,14]. The inter-ELM heat flux, ELM amplitude and frequency were chosen such that melting only occurred during the ELM transient itself, avoiding bulk melting. This occurred in a series of 5 consecutive, nearly identical discharges [15].

In this paper, we present a numerical study using the particle-in-cell (PIC) technique to estimate power deposition profiles on the side and top surfaces of the JET protruding lamella, combined with a simple 2D thermal model. The main aim being to understand heat fluxes expected on a protruding tile during large ELMs taking into account the Larmor gyration of the incoming ions and the consequent thermal response of the lamella. The different power flux scenarios in the simulations have been done by parameter scoping inside a range of experimental pedestal electron temperatures and densities to cover the ballpark of the expected energies carried by ELM pulses to the misaligned lamella. The numerical model used for heat flux calculation together with the geometry of the modeled lamella are presented in Section 2 of this article. Section 3 presents and discusses the results of the 2D power flux profiles on the protruding lamella surfaces, with the 2D thermal model and its application described Section 4. General conclusions are drawn in Section 5.

2. GEOMETRY AND NUMERICAL SET-UP

2.1. GEOMETRY

In the first part of the study, we focus on the expected power deposition profiles on the side of the misaligned JET lamella. The geometry of the experiment is shown in Figure 1, illustrating how the misalignment gradually increases in the poloidal direction, presenting a progressively higher edge to the parallel heat flux, which impinges essentially perpendicularly on the protruding edge. This special lamella is installed in a single module of the JET bulk tungsten outer divertor, in a poloidal location (on “Stack A” of the module comprising 4 separate stacks of lamellae) which is not wetted by the outer strike point during normal operation [16,17]. The lamella is 62mm long in the poloidal direction and 5.9mm wide in the toroidal direction. The degree of protrusion varies linearly from 0.25mm to 2.5mm across the poloidal extent. Several non-standard lamellas are also arranged toroidally just before the misaligned lamella to ensure that magnetic field lines are able to penetrate directly onto the misaligned edge (no self-shadowing).

2.2. Numerical set-up

Particle and power deposition profiles on perfectly aligned or misaligned monoblocks of castlellated PFCs can be simulated by means of PIC codes [12,18-20]. The electrostatic sheath and the magnetic pre-sheath, as well as the electric potential in the vicinity of the gaps between tiles play a major role in the plasma deposition in such geometry. At this geometric scale, the plasma is no longer quasi-neutral and the PIC technique can describe well the trajectories of charged particles in a self-consistent electric field. The code used here is a 2D-3V PIC code [21] which was developed at IPP Prague in collaboration with CEA Cadarache.

The electric field which accelerates the particles is derived from Poisson's equation at each time step. Ions are injected with an arbitrary velocity distribution function satisfying the Bohm criterion [22] and electrons are assumed to be Maxwellian. The case considered here is a fully ionized magnetized plasma with one species of singly charged ions (D^+) incident on a completely absorbing, conducting wall. The magnetic field can have arbitrary orientation and is assumed constant, which is true to a high approximation on the very short distances (few mm) appropriate to this experiment. A magnetic sheath [23,24] can thus develop along the surface in the range of $4*r_L$. This is accounted for here by ensuring a minimum distance of $10*r_L$ between the top of the protruding tile and the plasma-magnetic pre-sheath boundary, thus avoiding any perturbation to the bulk plasma. The extent of the lamella top surface in the toroidal direction is also taken large enough to avoid perturbations generated by the gap itself due to the periodicity of the system.

The two dimensionality of the code forces the modeled lamella to be semi-infinite in the poloidal direction with a constant protruding edge d with respect to the lamella (with a flat surface) directly in front of the special lamella (see Figure 2). In order to simulate the real situation, in which d varies poloidally, several simulations have been performed for different misalignments $d = 0.0, 0.5, 1.0, 1.5$ and $2.0mm$, implying a toroidal length of the simulation box ranging from 12–46mm to account for the shadowing from the protruding part on the reference tile due to the periodicity of the boundary conditions. PIC simulations are extremely time-consuming and have been performed on the supercomputer Helios in Rokkasho-Mura (Japan) on 16 processors. This limitation is due because of the Poisson solver not being parallelized. The duration of a single simulation varies between 3 and 12 weeks (CPU time) according to the size of the simulation box and the plasma conditions. For the maximum protruding edge of $2.5mm$, the simulation box was too large to be modeled in any realistic time. As it turned out, the real experiment did not push the strike point to the extreme location of highest misalignment and so such simulations are not necessary. Section 3 will show, however, that it is in fact straightforward to extrapolate the modeling results to larger values of d without performing the full PIC simulation.

The width of the gap between the lamella and its 2 neighbours is set to 1 mm, the toroidal magnetic field to $B_t = 2.5T$ (the experimental value at the radial position of stack A) and field lines impact the top surface with a shallow angle of $\alpha = 2.5^o$. Power deposition profiles are calculated on the side of the lamella (pink – Figure 2) and on the top surface (red – Figure 2). These two

surfaces will henceforth be referred to as the "side" and the "top" surfaces, respectively. These PIC simulations were conducted as part of the design of the JET lamella melting experiment and were thus performed before the actual experiment was conducted. The model input parameters were specified on the basis of set-up plasmas executed before the misaligned lamella was installed. The real plasma parameters used for the experiment (see Section 2.3) differed slightly from the values assumed in the model, but were sufficiently close for the model input to be equally valid for both the design phase and the interpretation of the experiments themselves.

2.3. ELM plasma parameter specification

During the experiment, transient ELM melting occurred during a sequence of five 3 MA pulses (JET Pulse No: 84778 to Pulse No: 84782) with a total additional heating power of 23 MW. The resulting H-mode plasma had about 6 MJ of total thermal energy and regular Type I ELMs with plasma energy loss of $\Delta W_{ELM} \sim 0.3$MJ. Within ~1s of the outer divertor strike point being placed on the misaligned lamella, the base temperature rose to values sufficient to allow transient melting at each ELM during the subsequent 0.5s. The lamella was monitored by local diagnostics including IR thermography systems.

Plasma conditions are implemented in the code via electron density (n_e) and ion/electron temperatures (T_i,T_e) at the sheath entrance. These local quantities cannot be measured reliably during Type I ELMs and so in the simulations 3 different power scenarios have been chosen on the basis of measured values of n_e and T_e in the H-mode pedestal (Figure 3), assuming that the ELM plasma impacting the divertor is characterized by these same parameters and that $T_i = T_e$.

The three different scenarios correspond to three chosen points in the measured pedestal profiles – at the top, middle and bottom of the pedestal. Table 1 summarizes the parameters, along with the resulting Larmor radius for D ions and the nominal parallel flux $q_{//,0}$. Figure 4 illustrates the IR measured temporal evolution of the parallel power density falling on the flat lamellas adjacent to the special, misaligned lamella during a single ELM. Experimental flux densities range from 0.1 GW/m^2 to 3 GW/m^2, values which are covered by the 3 numerical scenarios.

3. POWER FLUX DEPOSITION PROFILES DURING A SINGLE ELM

Figure 5 presents the PiC computed power flux density ($q_{//}^{PIC}$) profiles along the vertical edge of the misaligned lamella for the "least severe" case (S3) in Table 1. Two regions can be defined: negative x-axis values correspond to the protruding part of the special lamella, whilst positive x-values delimit the region inside the gap, thus below the level defined by the surface of the toroidally neighboring lamella which acts as the reference for the misalignment. For comparison, we have added on the graph the theoretical perpendicular power flux density which the top surface should see $q_{top\_surf} = q_{//,0}*sin(\alpha)$ and the almost parallel flux $q_{//} = q_{//,0}*cos(\alpha)$ (with $cos(\alpha) = 0.999$ for $\alpha = 2.5^o$) which would be expected to impact the side of the lamella in the absence of finite Larmor radius effects and simply assuming a guiding centre/ballistic approach with no electric field.

Inside the gap, the power deposition is rapidly damped decaying exponentially as already found in [25]. In the absence of finite Larmor radius effects, for a 1 mm gap, simple geometric projection would lead only to a penetration of 0.044mm down below the surface of the neighboring flat lamella. The PIC simulations predict that the deposited flux is lower than $q_{//}$ on the protruding side of the lamella, a consequence of the smoothing effect due to the Larmor gyration of the incoming ions [12]. For a 2 mm misalignment, 95% of $q_{//}$ is reached, but only $0.5q_{//}$ for a protruding edge of 0.5mm. As shown in [12], a surface perpendicular to field lines must protrude by at least $2r_L$ if the full parallel heat flux is to be intercepted.

This is further illustrated by Figure 6, which is the analog of Figure 5 but for the ELM scenario S1 in Table 1, with the highest ELM plasma temperature and hence the highest ion Larmor radius in the simulations. In this case, the smoothing effect increases, reducing the incident heat flux to 70% of $q_{//}$ at $d = 2mm$ and to only 35% at a misalignment of 0.5mm. By using the results of the full set of simulations (namely, the matrix of points obtained from the different values of d and ELM plasma temperature and density), a simple scaling law for the normalized heat flux deposited on the side of the lamella ($q_{//}^{PIC}/q_{//}$) as a function d normalized to r_L ($m = d/r_L$) can be derived. This scaling is shown in Figure 7 for the 3 ELM scenarios and is found to be linear ($q = a*m+b$), in the region of interest. These curves follow the same trend, even for different r_L. However, the contribution of the Larmor radius (and thus T_e) and n_e is also present in the coefficient a of the slope, which makes results difficult to extrapolate to other conditions and can explain the slight discrepancy observed between the curves. In Figure 7, the points corresponding to the maximum misalignment of the lamella ($d^{max} = 2.5mm$) are also displayed. For scenarios *S1* and *S2*, at most ~80% of $q_{//}$ would be expected for the highest misalignment, whilst for the ELM parameters of scenario *S3*, the parallel heat flux can actually be reached at full misalignment. It is important to note that simulations take no account of secondary electron emission (SEE). It has recently been shown [26] that for surfaces almost perpendicular to the magnetic field, SEE can have strong effects on the deposited power. The heat flux given here might thus be strongly underestimated. However, this will not change the ratio of deposited power to $q_{//}$ since SEE should affect the absolute values of all fluxes, including $q_{//}$.

The results for the calculated effective perpendicular power fluxes ($q_{\perp}^{PIC}$) falling on the top of the lamella for the ELM scenario *S3* are presented in Figure 8. The protruding lamella is located on the left of the gap for $y < 2.2mm$ (tile#2 on the schematic insert in Figure 8), with the reference lamella corresponding to all $y > 3.2mm$ (tile#1). Magnetic field lines impact from right to left. Due to the periodic boundary conditions used in the code, the modeled geometry is equivalent to having a virtual, second protruding lamella, next to the reference tile, as illustrated in the second schematic insert in Figure 8. Care must be taken in choosing the size of the simulation box and a sufficient length of tile#1 so as to avoid artificial shadowing at the point of interest, i.e. the gap and the protruding lamella. Due to the shallow angles, taking into account the entire box is too computationally intensive, so that the simulation domain is optimized such that the artificial shadowing occurs no further than 2mm before the gap entrance. This is why the deposited power flux on tile#1 for $y > 5mm$ is lower

than the nominal flux when the tiles are well aligned (here $q_{top\_surf} = 8\ MW/m^2$).

There is clearly an enhanced heat flux on the top surface of the misaligned lamella in comparison to the geometrically expected value. Moreover, the top surface heat flux profile peaks near the misaligned corner, with the degree of peaking increasing with increasing misalignment. The effect is due to the perturbation caused by the protruding edge, creating local electric fields which increase with increasing protrusion and attract ions (see Figure 9). The toroidal electric field (E_y) on the side of the lamella for a maximum misalignment of 2mm (Figure 9 – left) is increased by a factor 3 from its value at the entrance of the gap (reference), whilst the radial electric field (E_z) on the top of a 2mm protruding lamella (Figure 9 – right) is of same order of magnitude. Although this effect can considerably enhance the top surface power flux density over that expected geometrically (by up to a factor 7.5 in Figure 8), it is still a small fraction of the parallel heat flux which is deposited on the lamella side, near the corner (Figure 5). A simple power balance shows that the missing power is redeposited on the top of the protruding tile. For scenario S3 and in the case of no misalignment, the integral of the power falling in the 1mm gap is 8 W/mm. From Figure 5, the integral of the power falling inside the gap (over ~0.5 mm) gives ~3 W/mm, to what should be added the integral of the peaked power just at the corner of the protruding tile, which is found to be 5W/mm. Similar confirmations have been performed for the 4 protruding cases. A similar trend is found for ELM plasma cases *S1*, *S2* and a scaling can be defined for the top surface power deposition enhancement in a similar fashion to that performed for the side heat fluxes. Figure 10 shows the lamella top deposition power flux profiles normalized to q_{top_surf} as a function of the distance from the top surface normalized to the r_L ($n = y/r_L$) for scenario *S2* and for 5 simulated misalignments. The edge of the lamella corresponds to $n = 0$ and so that increasing n corresponds to increasing distance from the gap/edge.

The power deposition along the top surface clearly decreases with a double exponential decay. The first region corresponds to the peak value near the corner, in between points A and B on the graph. It has a short decay length, λ_{short}, over a distance $0.4r_L$ from the edge. The second region corresponds to broader profiles with a much larger decay length, λ_{long}, for the rest of the lamella top, between points B and C. The picture is similar for all the simulated scenarios, with $\lambda_{short} \sim 0.4r_L$. The power deposition profiles can thus more generally be characterized by the value of the peak at the corner, i.e. point A, and λ_{short}. The long decay length varies from 20 – 300 r_L and thus is essentially flat given the small extent of the lamella width (~$6r_L$ for ELM scenario *S3*).

Since the short decay length is constant for all the simulations ($\lambda_{short} = 0.55 \pm 0.02$) a scaling law is required only for the peaked top heat flux at the corner. The normalized power flux density peak near the edge is plotted as a function of normalized misalignment for all ELM scenarios in Figure 11. It varies linearly with the misalignment and is similar for all ELM cases.

Having determined approximate scalings for the deposited heat flux on the misaligned lamella contour, the temporal evolution of the surface temperature can now be obtained by solving the heat equation. This is described in the following section.

4. TEMPORAL EVOLUTION OF SURFACE TEMPERATURE DURING ELMS

4.1. THE 2D THERMAL MODEL

A 2D thermal model has been developed in the same 2D PIC geometric coordinates (with an infinite poloidal dimension) to address the temperature rise on the inertially cooled, misaligned lamella due to the PIC computed power flux densities. It solves the standard heat equation, where T is the temperature (in this case a two-dimensional matrix with time-dependent elements) and $\alpha = k/\rho c_p$ the temperature independent thermal diffusivity (k = thermal conductivity, c_p = specific heat capacity, ρ = density) calculated with the following W properties: $k = 173\ W/(m.K)$, $c_p = 130\ J/(kg.K)$, $\rho = 19250 kg/m^3$ and the melting temperature is set at $T^{melt} = 3695K$. The variable q is the net external heat source, provided here by the PIC simulations. A discrete square grid and a finite difference numerical method are used, as well as an implicit scheme to solve the sparse matrix-defined system of linear equations. We assume that no other energy sources or radiation losses are present in the lamella. The heat equation defines a sparse matrix when $T(t, x, y)$ is treated as a time-dependent vector with n_x x n_y elements. At the boundaries, the temperature is maintained constant. Since the PIC output is in the form of a surface heat flux, the flux q is related to the energy flux Q_S coming from the plasma through the surface of the grid element S, by $q(x, y) = Q_S(x, y)*S/(m*c_p)$, with m the mass of 1 cell, assuming a stationary flux. The temperature in the empty space beneath the boundary of the tile material is taken constant in the direction of the flux (simulating conductive cooling of the lamella). The model is simple in comparison with commercial 3D finite-element solvers, but can be run rapidly and provides trends, which have been well reproduced by a more complete numerical thermal model during transients (ELMs) [27].

4.2. TEMPORAL EVOLUTION OF SURFACE TEMPERATURE PROFILES

The surface temperature of the lamella (T^{surf}) is calculated during ELMs using the PIC power flux profiles presented in section 3. The temporal evolution of the ELM power flux density is modeled by the function shown in Figure 12, which corresponds to the conditionally averaged IR measured profile during the transient melt experiments. The starting temperature of the lamella (T^{base}) is a free parameter, set arbitrarily to 2700K here. During the experiment, the nominal strike point position was at a poloidal location corresponding to a height of $d = 1.5mm$ on the special lamella so power fluxes from the PIC simulations for this level of misalignment are used. Spatial profiles of T^{surf} on both surfaces of the lamella are presented in Figure 13 for the ELM scenario S2, for which the Larmor smoothing, $q^{PIC}/q_{//} = 0.6$ on the protruding edge (see Figure 7 for $m = \sim 1$). Under these conditions, the thermal model finds that the melting point is reached 1 ms after the start of the ELM.

Unsurprisingly, the lamella temperature profile reflects the PIC power deposition and is more strongly heated on the protruding edge (Figure 13 – left), with the temperature increasing towards the corner (there is a gradient of $\Delta T^{side} \sim 400K$ over 1.5mm for the maximum time). In contrast, the top surface temperature remains essentially constant except for the strong peaking at the corner (point B in Figure 13) where there is again a strong gradient ($\Delta T^{top,corner} \sim 450K$) within 0.5 mm (Figure

13 – right), reflecting the peaked power deposition in Figure 8, but also the very high power flux density incident on the protruding edge (of much higher magnitude than the top surface power flux density). In fact, the power falling on the top surface after the full 1 ms ELM duration accounts for only 100K of the total temperature increase at the corner.

For comparison, results for the ballistic case, without Larmor smoothing and using the nominal parallel flux $q_{//,0}*cos(\alpha)$ and $q_{//,0}*sin(\alpha)$ on the side and top surfaces, respectively are shown in Figure 14.

In this case, the peak temperature increase at the top-side corner, $\Delta T^{top,corner} \sim 950K$ over a distance 0.5mm at the end of the ELM event is twice the PIC case. There is also a much smaller (~100K) temperature increase at the side-corner, due to the additional contribution from the perpendicular flux at the top always present at this transitional location. The key difference between the PIC and geometrically projected power flux cases lies with the absolute values of T^{surf}. The temperature rise on the protruding edge from the base temperature in the ballistic case is ~600K higher that the spatially averaged PIC and is a clear demonstration of the Larmor smoothing effect. The corner temperature follows the same trend. Figure 15 plots the temporal evolution of the temperature at the hottest point on the lamella during the ELM is plotted for both PIC and ballistic cases.

The same trend is found for all three simulated ELM cases and even in the case of *S3*, in which melting does not occur, the difference in the corner temperature follows the power flux Larmor smoothing. The main difference is found in the spatial distribution of T^{surf} along the protruding edge,(Figures 13 and 14), but from the point of view of melting, the important point to monitor is the corner where a sharp rise of T^{surf} is observed. Here, the total flux is a combination of the parallel and perpendicular components and corresponds to the maximum flux, independently of the heat flux spatial distribution further from this point. In the PIC case, the perpendicular flux is enhanced with respect to the theoretically expected value based on an optical projection. The absolute value depends on the particular geometry (magnitude of the protruding edge) and the plasma scenario (Larmor radius) and must be assessed more generally for all cases including contributions from both the side and top.

A scaling for the total heat flux falling on the corner can be derived as a function of the misalignment normalized to r_L. At the corner, the total incoming flux in both the PIC and ballistic cases (Figures 5 and 8) satisfies the following equation:

$$q_{//,0}*cos(\alpha) + q_{//,0}*sin(\alpha)\ (= q_{//} + q_{top\_surf}) \approx q_{//}^{PIC} + q_{\perp}^{PIC}, \quad (1)$$

with $q_{//}^{PIC}$ and $q_{\perp}^{PIC}$ being the power fluxes given by the PIC calculations falling on the side and top, respectively.

Using the scaling formulas given in Figures 7 and 11 for the side and top profiles, the flux falling on the corner normalized to q// can be described as follows:

$$\boldsymbol{q^{corner}/q_{//} = q_{//}^{PIC}/q_{//} + (q_{\perp}^{PIC}/qt_{op\_surf})*sin\ (\alpha)} \quad (2)$$

and is shown in Figure 16 for the 3 ELM cases. The curves have a linear dependence until they reach the limit value of $q_{//}$, which is the maximum energy available in the system. Values greater than unity (grey area) are therefore non-physical and the power flux falling at the corner is thus $q_{//}$. The corner flux is at best $\sim 0.4 q_{//}$ for the smallest experimental misalignment ($d^{min} = 0.25mm \rightarrow m \sim 0$) for all scenarios. For scenarios *S1 & S2*, curves reach the nominal parallel flux for a misalignment $d > 2mm$, but for the experimental misalignment of $d = 1.5mm$ (squares in Figure 16), points lie in the region where the Larmor smoothing is effective (~ 80%). For scenario S3, even for the experimental misalignment, the corner experiences the full parallel flux and does not benefit from any smoothing effect for a misalignment greater than 1.3mm ($m = 1.6$). Such low energy ELMs are, however, unlikely to melt the W lamella.

The PIC calculations define two regions with respect to the finite misalignment of the lamella where the corner fully benefit from the Larmor smoothing effect with a reduced heat flux or not by experiencing the full parallel flux. However, this corresponds to an ideal case in which the corner is sharp and in which there is no change in the geometry with time. In reality, due to the high fluxes and the initial sharp edge, melt erosion of the corner occurred rapidly after only a few ELMs [13,14], modifying the perpendicular geometry and hence magnetic field line impact. The values presented in Figure 16 should thus be taken as upper limits and it is reasonable to expect in reality that the smoothing effect should be more slightly more efficient as edges become rounded under plasma exposure.

5. CONCLUSIONS

In support of a proposal by the ITER Organization to eliminate the planned CFC/W divertor and begin operation with a full W divertor, an experiment has been executed on the JET tokamak to investigate the dynamics of ELM-induced transient melting on a deliberately misaligned W lamella in the bulk W outer divertor target [13,14]. Prior to the experiment, a series of 2D particle-in-cell simulations were performed to assess the potential benefit which might be expected due to the Larmor radius smoothing effect which is expected to modify the power flux deposition in the vicinity of misaligned edges [12]. The input parameters for these simulations were chosen based on experimental data obtained in similar H-mode discharges to those executed during the real experiment and were subsequently confirmed to be appropriate to the experiment itself.

As in earlier work [12], the new simulations reported here demonstrate that the power deposition profiles on the protruding side of the lamella are lower than the expected parallel flux thanks to the Larmor smoothing effect which is effective when the edge is misaligned by a distance lower than $2r_L$. In contrast, on the top surface of the misaligned lamella, the power deposition profiles are higher than geometrically expected. This is because the deficit of power on the protruding edge is deposited on the top surface as a result of the strong electric fields which develop along the protruding surface, as it is proven by a power balance. The corner of the lamella receives the highest heat flux and this is then naturally the point at which melting would be expected to begin for sufficiently energetic ELMs.

Scaling laws have been derived to describe the power deposition profiles for both the protruding and top surfaces, and therefore at the corner, as a function of the protruding distance normalized to the Larmor radius. Profiles are linear and thus independent of the ELM conditions assumed in this study. The corner power flux density falls into one of two categories: a beneficial Larmor smoothing effect (for large ELMs and small edges) or a situation in which there is no benefit and the corner experiences the full parallel flux (for small ELMs and greater protrusion). Thermal analysis using a 2D finite difference code to solve the time dependent heat equation shows that despite the enhanced top surface heat flux, the corner temperature is only slightly affected compared to a case where there is no additional power on the top and he temperature curves at the corner seem to follow the side Larmor smoothing scaling.

This numerical study demonstrates that in the presence of small misalignments a competition exists between more energetic ELMs with a large smoothing effect (higher Larmor radius) and smaller ELMs for which the orbit effects are effectively absent.

ACKNOWLEDGMENTS

The authors would like to acknowledge Dr. Ph. Mertens for detailed description of the special misaligned lamella geometry, and Dr. Y. Corre and Dr. B. Bazylev for fruitful discussions on surface temperature data interpretation from both the experimental and numerical simulation points of view.

This work, part-funded by the European Communities under the contract of Association between EURATOM/IPP.CR was carried out within the framework of the European Fusion Development Agreement. The views and opinions expressed herein do not necessarily reflect those of the European Commission or those of the European Commission or of the ITER Organization.

REFERENCES

[1]. Pitts R A et al., Journal of Nuclear Materials **415** (2011) pp. S957–S964
[2]. Kreiger K et al., Physica Scripta **T145** (2011) 014067
[3]. Coenen J W et al., Journal of Nuclear Materials **438** (2013) S27
[4]. Lipschultz B et al., Nuclear Fusion **52** (2012) 123002
[5]. Bazilev B et al., Physica Scripta **T145** (2011) 014054
[6]. Miloshevsky G and Hassanein A, Nuclear Fusion **54** (2014) 033008
[7]. Neu R et al., Plasma Physics and Controlled Fusion **53**, no. 12 (2011) 124040
[8]. Neu R, IEEE Transactions on Plasma Science, Vol. **38**, No. 3, March 2010, pp. 453–460
[9]. Thomser C et al., Fusion Science and Technology **62**, No. 1 (2012) pp. 1–8
[10]. Matthews G F et al., Journal of Nuclear Materials **438** (2013) pp. S2–S10
[11]. Missirlian M et al., Fusion Engineering and Design (2014) http://dx.doi.org/10.1016/j.fusengdes.2014.01.050
[12]. Dejarnac R et al., Journal of Nuclear Materials **415** (2011) pp. S977–S980

[13]. Coenen J W et al., *'ELM induced W melting and its impact on tokamak operation'*, invited paper at the 21st International Conference on Plasma Surface Interactions, May 2014
[14]. Matthews G F et al., '*Melting of Tungsten by ELM Heat Loads in the JET Divertor',* paper submitted to the 25th IAEA Fusion Energy Conference, October 2014.
[15]. Arnoux G et al., *'Thermal response up to melting of the exposed edge of a W lamella in the JET divertor',* to be presented at the 21st International Conference on Plasma Surface Interactions, May 2014
[16]. Mertens P et al., Journal of Nuclear Materials **415** (2011) pp. S943–S947
[17]. Mertens P, Physica Scripta **T145** (2011) 014002 (7pp)
[18]. Dejarnac R et al., IEEE Transactions on Plasma Science, Vol. **38**, No. 4, April 2010, pp. 1042–1046
[19]. Komm M et al., Plasma Physics and Controlled Fusion **53** (2011) 115004
[20]. Komm M et al., Plasma Physics and Controlled Fusion **55** (2013) 025006
[21]. Dejarnac R et al., Journal of Nuclear Materials **363–365** (2007) pp. 560–564
[22]. Gunn J P, Journal of Nuclear Materials **337–339** (2005) p. 310
[23]. Chodura R, Physics of Fluids **25** (1982) p. 1628
[24]. Gunn J P, Physics of Plasmas **4** (1997) p. 4435
[25]. Dejarnac R et al., Journal of Nuclear Materials **390–391** (2009) pp. 818–821
[26]. Gunn J P, Plasma Physics and Controlled Fusion **54** (2012) 085007
[27]. Bazylev B, *Private communication*

	$n_e[m^{-3}]$	$T_e = T_i[eV]$	$r_L[mm]$	$q_{//,0}[GW/m^2]$
Scenario 1 *(S1)*	7.10^{19}	*500*	*1.8*	*7.10*
Scenario 2 *(S2)*	4.10^{19}	*300*	*1.4*	*1.90*
Scenario 3 *(S3)*	2.10^{19}	*100*	*0.8*	*0.18*

Table 1: Summary of the three different ELM scenarios simulated with given input density and temperatures and resulting Larmor radius (r_L) and nominal parallel flux ($q_{//,0}$)

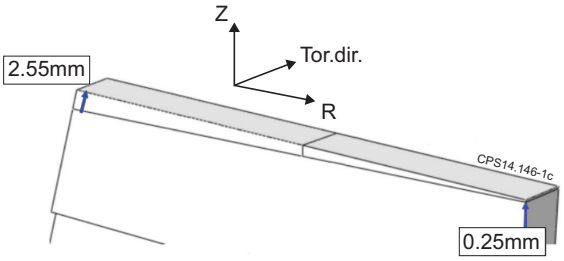

Figure 1: Schematic of the special protruding lamella in the JET divertor.

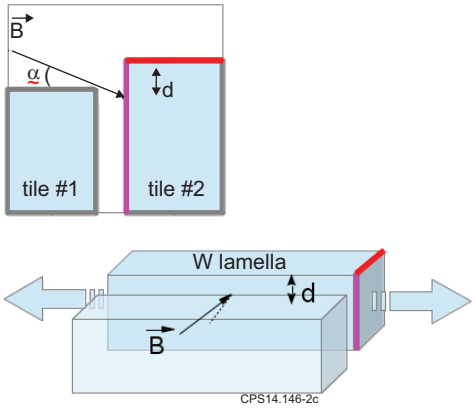

Figure 2: Schematic of the (semi-infinite) lamella as modeled in the 2D PIC simulations.

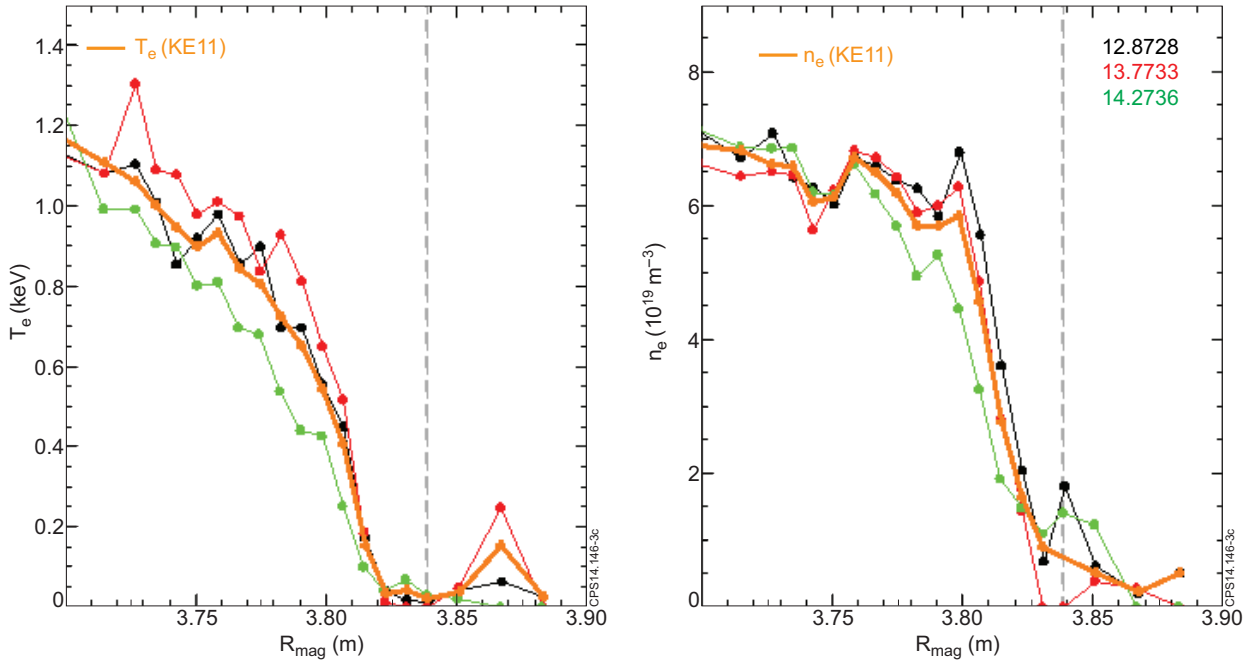

Figure 3: Thomson scattering pedestal profiles of T_e (left) and n_e (right) at 3 different times from one discharge (JET Pulse No: 84781) in the series of five repeated pulses during which transient melting occurred on the misaligned lamella.

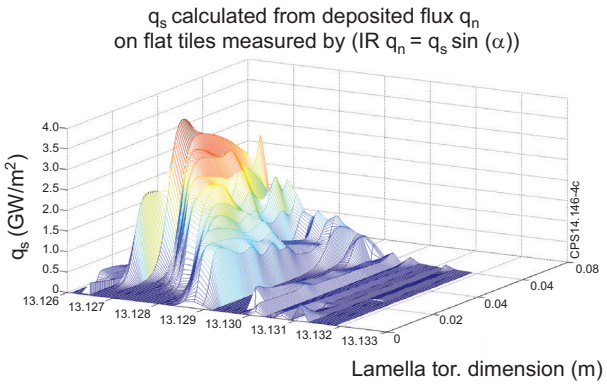

Figure 4: Temporal evolution of the spatial distribution of the power density falling on a flat lamella adjacent to the misaligned lamela during a single ELM, measured by IR thermography in 1 of the 5 melting discharges (JET Pulse No: 84779).

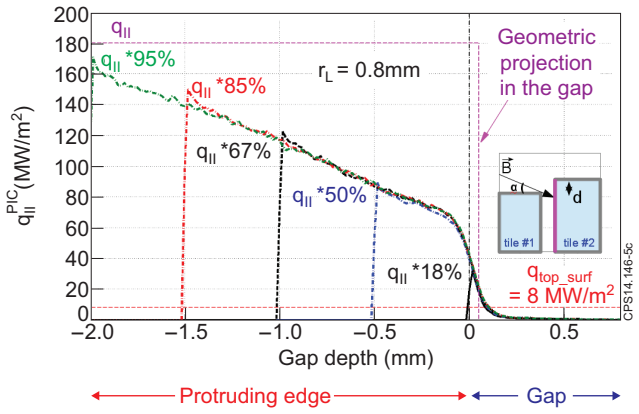

Figure 5: Power deposition profiles along the misaligned lamella side (including down below the surface defined by the neighboring lamella) for scenario S3 and 5 simulated misalignments. The theoretically expected power fluxes on the top surface and the parallel heat flux in the absence of any finite Larmor radius effects are marked for comparison.

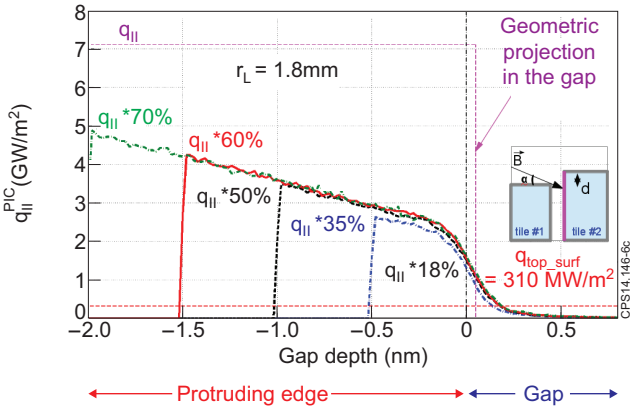

Figure 6: As for Figure 5 but for scenario S1.

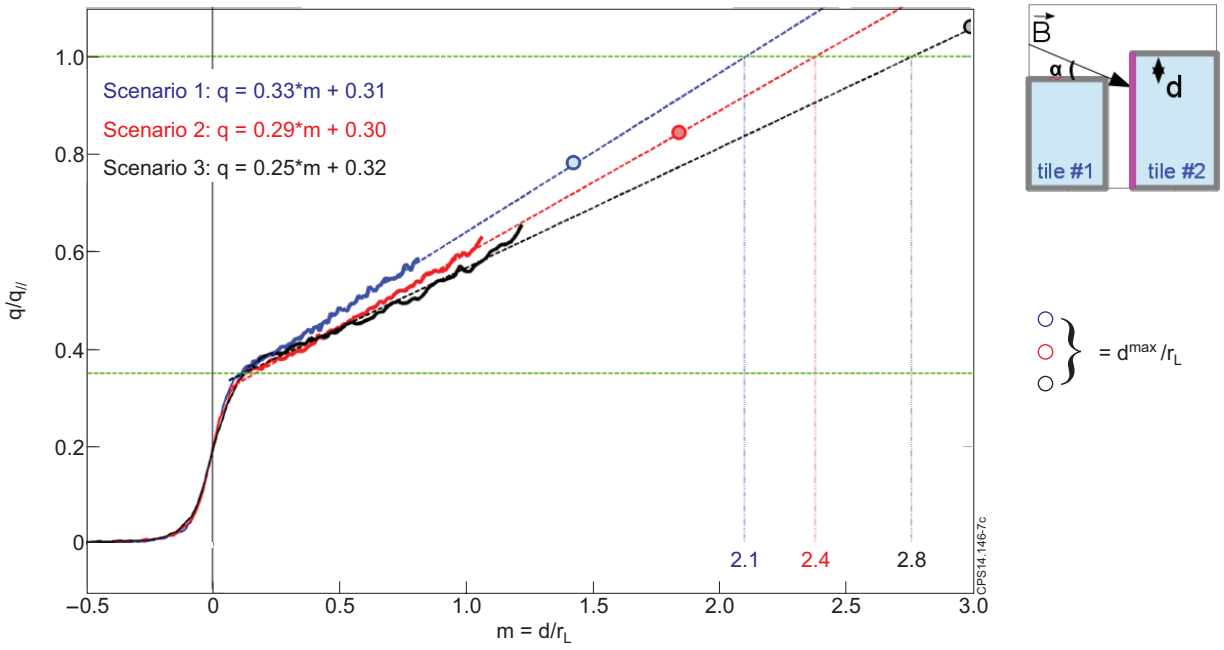

Figure 7: Scaling of the power deposition profiles on the side of the misaligned lamella (normalized to $q_{//}$) as a function of the misalignment normalized to r_L.

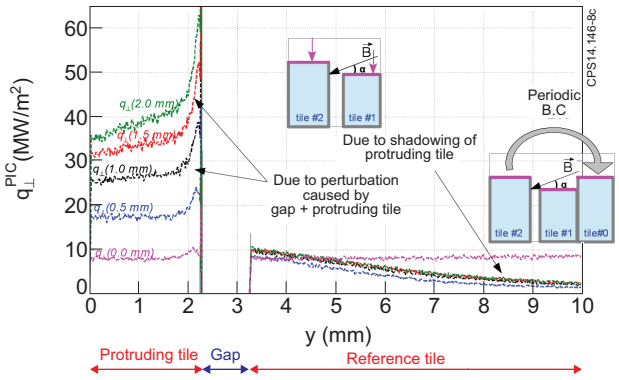

Figure 8: Power deposition profiles on the top surface of the misaligned lamella for scenario S3 and the 5 simulated misalignments (only 10 mm in the toroidal direction are shown).

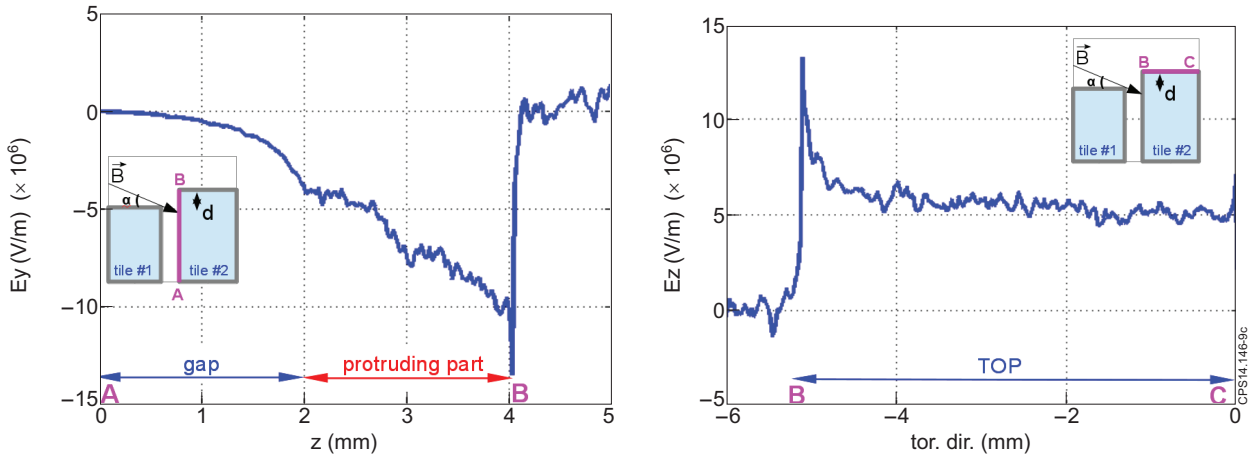

Figure 9: Toroidal electric field at the side (left) and radial electric field at the top (right) of the lamella for a 2mm protruding lamella in scenario S2 computed by 2D PIC calculations.

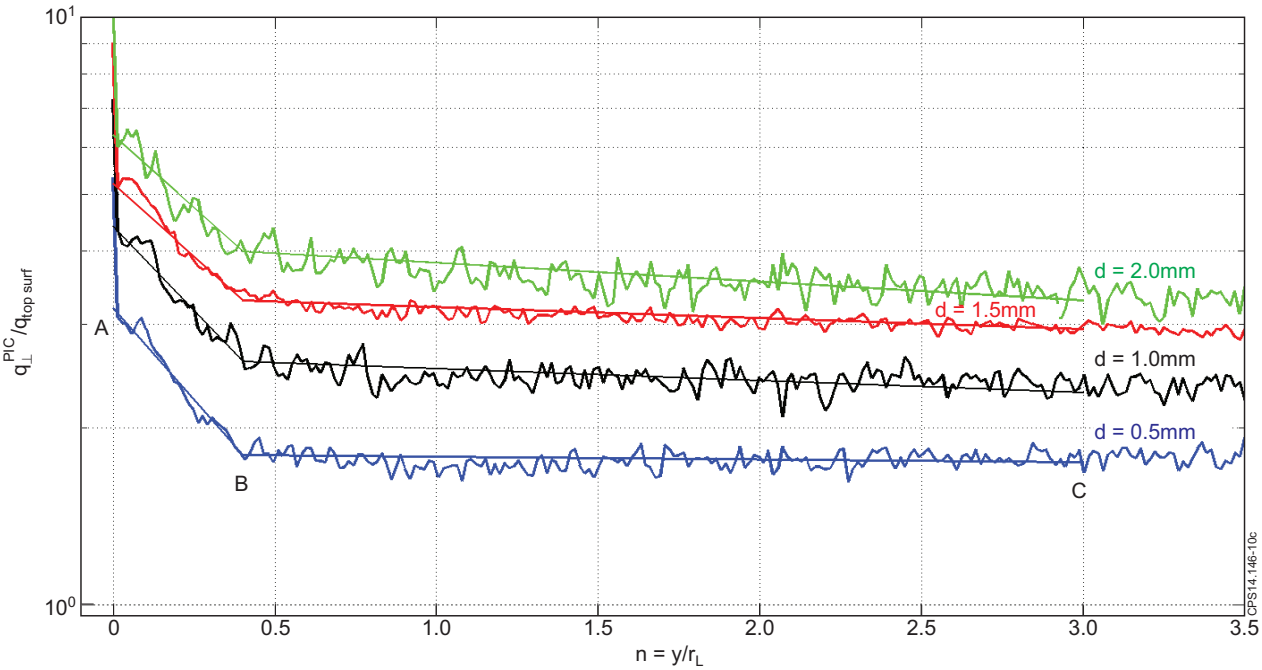

Figure 10: Spatial profiles of the power flux deposition normalized to q_{top_surf} as a function of the distance normalized to r_L on the top surface of the lamella for ELM scenario S2 and 4 simulated misalignments.

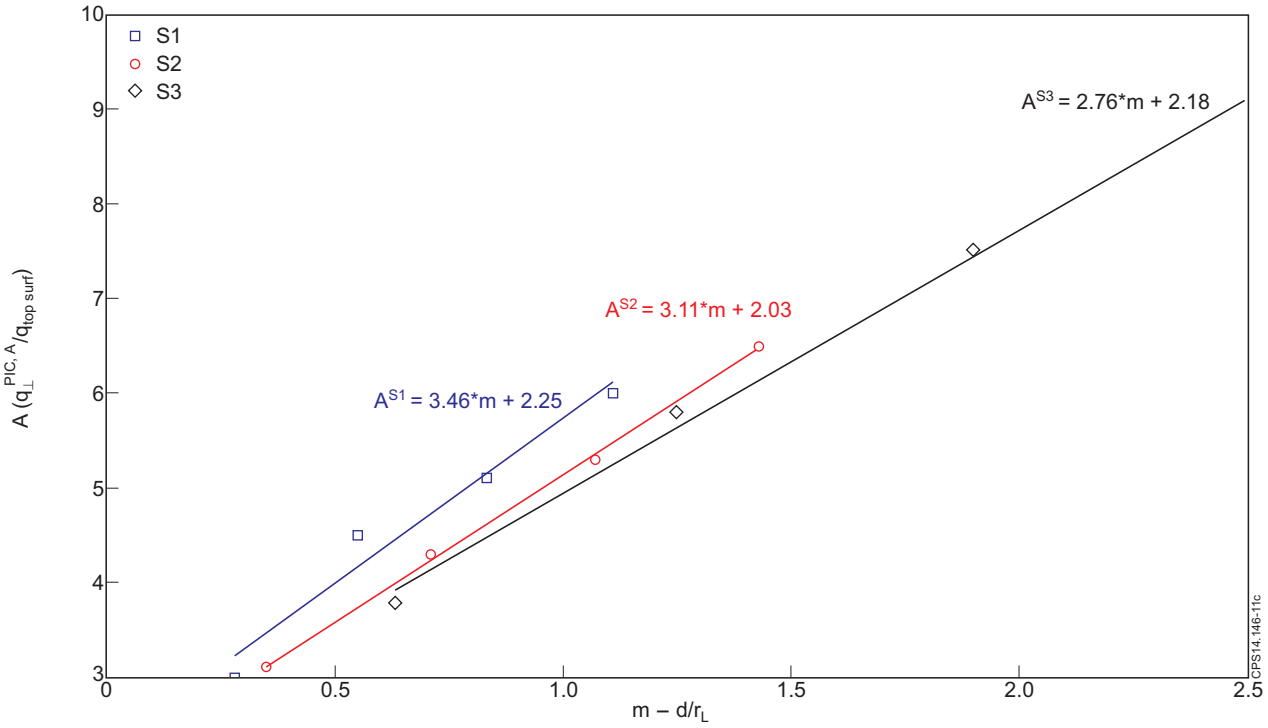

Figure 11: Scaling law for the peak value of the deposited power flux normalized to q_{top_surf} as a function of the misalignment normalized to r_L on the top surface of the misaligned lamella for the 3 ELM cases.

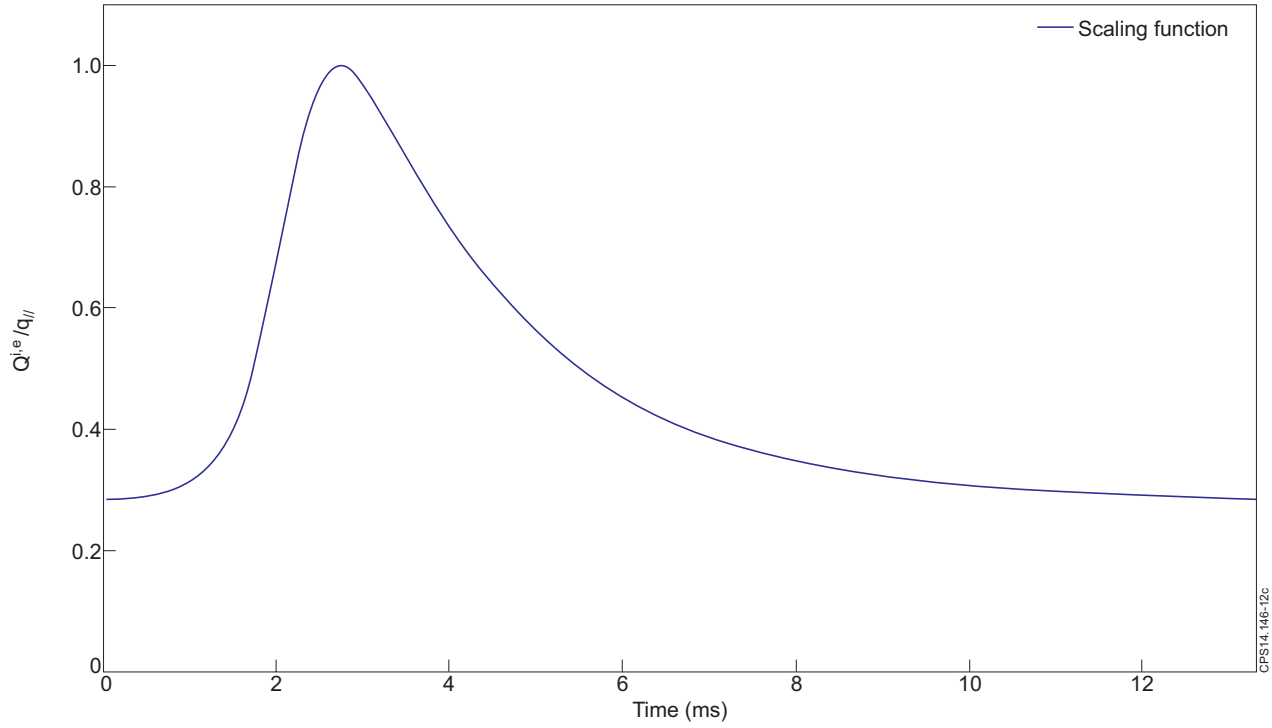

Figure 12: Temporal evolution of the normalized power flux for 1 ELM in JET.

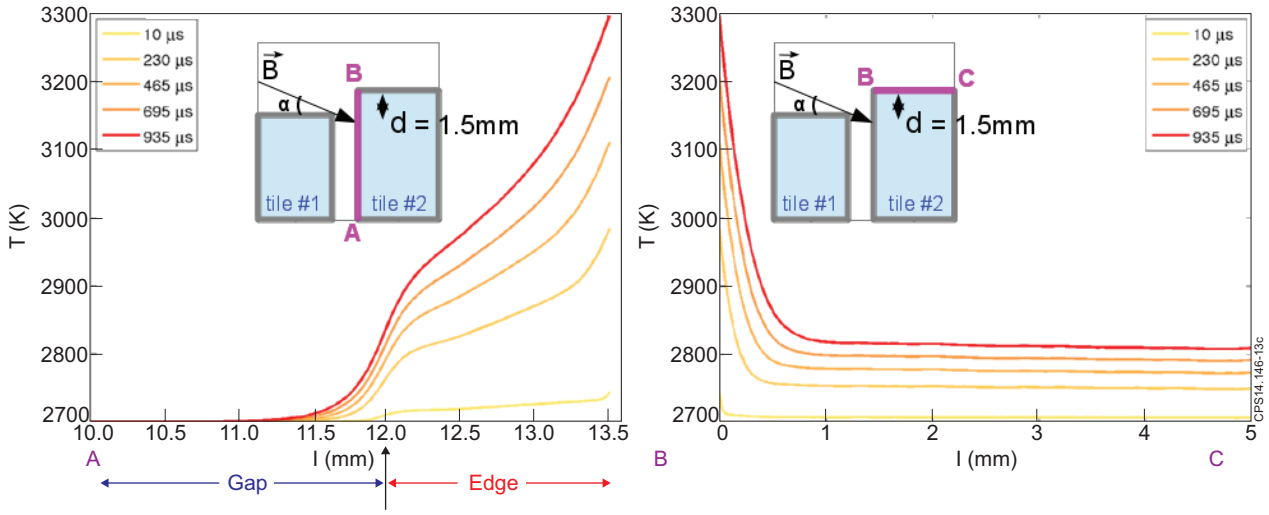

Figure 13: Spatial profiles of the surface temperature on the side (left) and top (right) of the misaligned lamella at different times during the ELM (Scenario S2) and for a misalignment of d = 1.5mm.

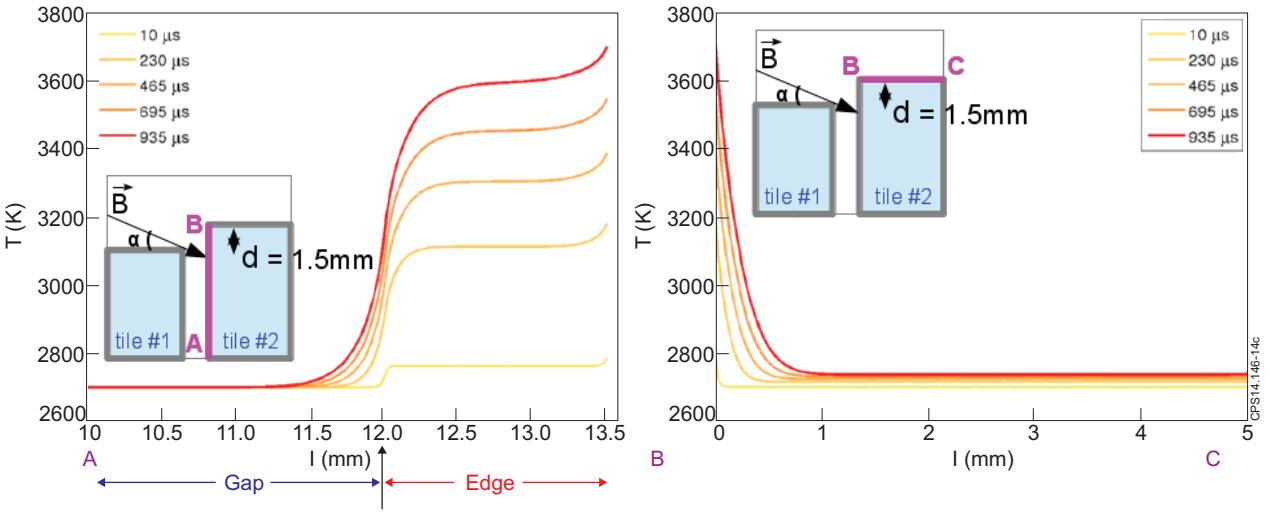

Figure 14: Analog of Figure 13, but using geometrically projected input heat fluxes.

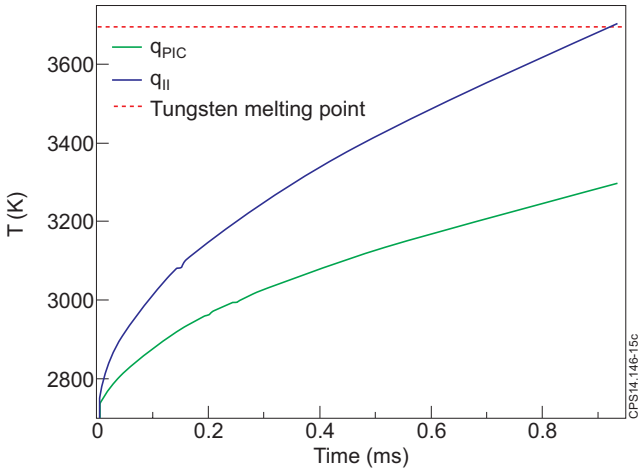

Figure 15: Temporal evolution during the ELM of T^{surf} at the hottest point on the special lamella for the ballistic (green) and PIC (blue) power fluxes (scenario S2 and d = 1.5mm).

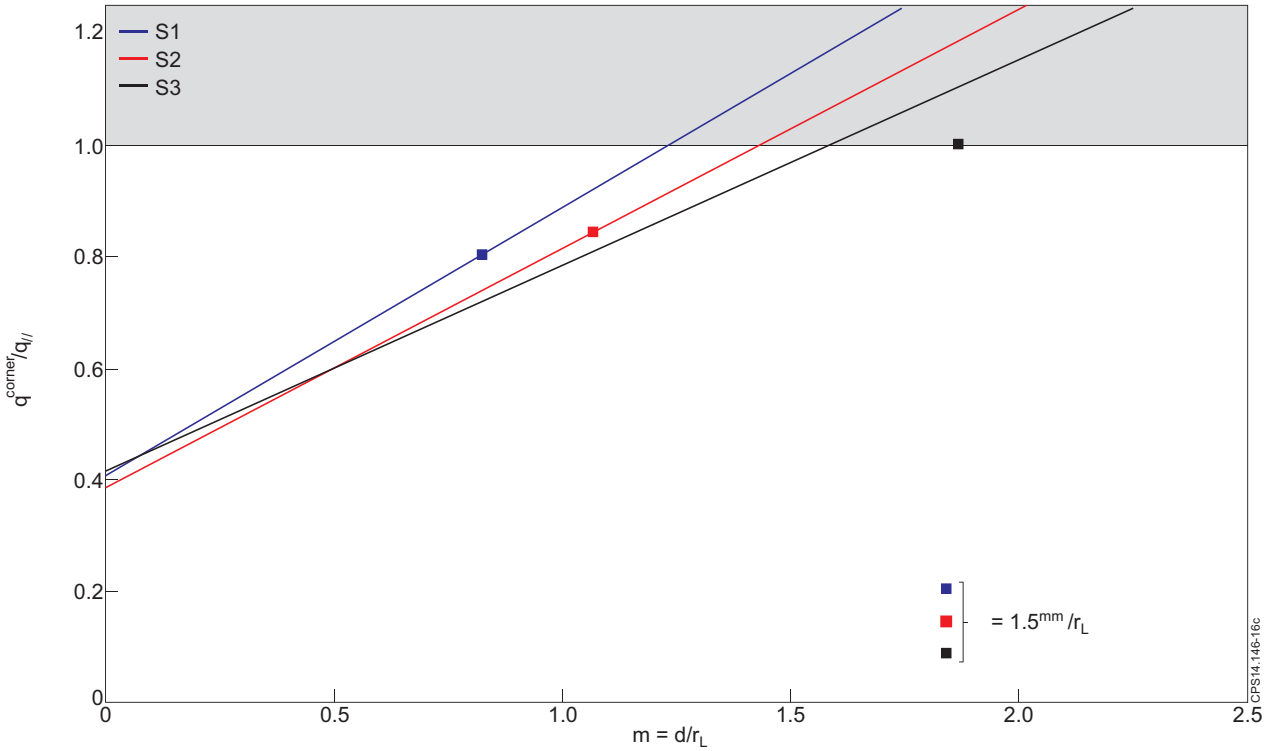

Figure 16: Scaling law for the power flux normalized to $q_{//}$ falling on the corner of the special lamella for different ELM scenarios as a function of the misalignment normalized to r_L.